symmetry

Article

The Rotor-Vibrator Plus Multi-Particle-Hole Description of ^{154}Gd

Yingxin Wu [1], Aoxue Li [1], Feng Pan [1,*], Lianrong Dai [2] and Jerry P. Draayer [3]

1 Department of Physics, Liaoning Normal University, Dalian 116029, China
2 Department of Physics, School of Science, Huzhou University, Huzhou 313000, China
3 Department of Physics and Astronomy, Louisiana State University, Baton Rouge, LA 70803-4001, USA
* Correspondence: daipan@dlut.edu.cn

Abstract: Based on the well-known rotor-vibrator model and the particle-plus-rotor model, multi-particle-hole excitations from a collective even-even core described by the rotor-vibrator is considered to describe well-deformed even-even nuclei. Like the particle-plus-rotor model, the intrinsic Vierergruppe (D_2) symmetry is still preserved in the rotor-vibrator plus multi-particle-hole description. It is shown that a series of experimentally observed 0^+ states in these nuclei may be interpreted as the multi-particle-hole excitations in a complementary manner to the beta and gamma vibrations described by the rotor-vibrator model. As a typical example of the model application, low-lying positive parity level energies below 1.990 MeV in the eight experimentally identified positive parity bands; a series of 0^+ excitation energies up to 0^+_{16}; and some experimentally known B(E2) values, E2 branching ratios, and E2/M1 and E0/E2 mixing ratios of ^{154}Gd are fitted and compared to the experimental data. The results suggest that the multi-particle-hole-pair configuration mixing may play a role in these 0^+ states.

Keywords: rotor-vibrator; multi-particle-hole excitation; configuration mixing; well-deformed nuclei

PACS: 21.10.Re; 21.60.Ev

check for updates

Citation: Wu, Y.; Li, A.; Pan, F.; Dai, L.; Draayer, J.P. The Rotor-Vibrator Plus Multi-Particle-Hole Description of ^{154}Gd. *Symmetry* **2022**, *14*, 2620. https://doi.org/10.3390/sym14122620

Academic Editor: Andrea Lavagno

Received: 15 November 2022
Accepted: 6 December 2022
Published: 10 December 2022

1. Introduction

As is well known, both the collective model and the interacting boson model (IBM) are very successful in describing spectroscopy of medium and heavy mass nuclei in low-energy regime [1,2]. Shape phase evolution in these nuclei has also been extensively studied [3–8]. Shell model description of deformed nuclei has also been studied extensively [9–11] based on the pseudo SU(3) model [12–14]. Up until now, most studies on low-lying spectra of deformed nuclei in both rare earth and actinide regions have focused on a few low-lying bands [15–23]. In [9–11], besides several low-lying bands, strongly enhanced M1 strengths and related 1^+ states were focused. However, it can be observed from the experimental data of these well-deformed nuclei, typically in even-even $^{154-160}$Gd, that there are many 0^+ excited states populated below 3 MeV, which is also related to the long-term debate on the nature of the low-lying 0^+ states [24–27]. Nevertheless, these 0^+ states have not been fully taken into account in model calculations [15–23].

Although rigorous shell model calculations with configuration mixing are needed in order to reveal the nature of the 0^+ states, the collective rotation–vibration model (RVM) [28] is the simplest, at least qualitatively, to describe the low-lying rotational bands, such as the ground-state, beta-, and gamma-vibration bands; although, these 0^+ states described by the RVM are questionable with too high excitation energies of 0^+_u levels with $u \geq 4$ compared to the corresponding experimental data [29]. Moreover, the particle-plus-rotor model (PRM) [1,30–34] is often adopted to describe well-deformed odd-A and odd-odd nuclei, where the rotor is used to describe the collective motion of the even-even core, while the deformed Nilsson model is used to describe the concerned like-particles. As an extension, in this work, we consider particle-hole excitations from the collective even-even core, with which the 0^+ and other bands are modified by the multi-particle-hole excitations. Although the model Hamiltonian proposed can be applied to any well-deformed nucleus, only ^{154}Gd is taken as an example in the fit, of which the main features persist when the model is applied to other deformed nuclei.

2. Formalism

We take the RVM Hamiltonian for the core of a well-deformed even-even nucleus. Instead of the RVM Hamiltonian, one can also use the Davydov–Chaban version of the collective Hamiltonian [35], of which, however, the main features are quite similar to those of the RVM. According to the PRM prescription [1,30–34], the Hamiltonian with configuration mixing due to multi-particle-hole excitations from the core is approximated as

$$\hat{H} = P\left(\hat{H}_{\mathrm{RV}} + \hat{H}_{\mathrm{in}}^{\mathrm{pro}} + \hat{H}_{\mathrm{in}}^{\mathrm{n}}\right)P, \tag{1}$$

where $\hat{H}_{\mathrm{RV}}$ is the RVM Hamiltonian, which is approximated to be the same when a few particles and holes are excited from the core for simplicity; $\hat{H}_{\mathrm{in}}^{\mathrm{pro}}$ ($\hat{H}_{\mathrm{in}}^{\mathrm{n}}$) contains proton (neutron), single-particle (p), and single-hole (h) energy terms and the interaction among $K = 0$ like-particle and like-hole pairs due to the fact that the nuclear shape described by the RVM is approximately axially symmetric, where K is the quantum number of the projection of the angular momentum along the third axis of the intrinsic frame and P is the projection operator, which projects onto 0p0h, 2p2h and 1p1h, 3p3h even parity $K = 0$ subspace of protons and neutrons. Namely, as an approximation, only 2p2h excitations established on the 0p0h and 1p1h basis of protons and neutrons are considered. The RVM Hamiltonian is given by [25,28]

$$\hat{H}_{\mathrm{RV}} = \frac{L^2 - L_{z'}^2}{2\Im_0} + \frac{L_{z'}^2}{16B\eta^2} - \frac{\hbar^2}{2B}\left(\frac{\partial^2}{\partial\xi^2} + \frac{1}{2}\frac{\partial^2}{\partial\eta^2}\right) + \frac{1}{2}C_0\xi^2 + C_2\eta^2 - \frac{\hbar^2}{16B\eta^2}, \tag{2}$$

where B is the inertia parameter; C_0 and C_2 are the stiffness parameters; $\Im_0 = 3B\beta_0^2$ is the moment of inertia, in which β_0 is the deformation parameter; L_τ with $\tau = x', y', z'$ are the angular momentum operators of the core in the intrinsic frame; and ξ and η are variables in describing small β and γ vibrations. $\hat{H}_{\mathrm{in}}^{\mathrm{pro}}$ and $\hat{H}_{\mathrm{in}}^{\mathrm{n}}$ are given by

$$\hat{H}_{\mathrm{in}}^{\mathrm{pro}} = \sum_{i=1}^{p_{\mathrm{pro}}} \varepsilon_{i,\,\Omega_i}^{\mathrm{pro}}\,\hat{n}_{i,\,\Omega_i}^{\mathrm{pro}} - \sum_{i'=-p'_{\mathrm{pro}}+1}^{0} \varepsilon_{-i',\,\Omega_{-i'}}^{\mathrm{pro}}\,\hat{n}_{-i',\,\Omega_{-i'}}^{\mathrm{pro}} + g_{\mathrm{pro}} \sum_{i=1}^{p_{\mathrm{pro}}} \sum_{i'=-p'_{\mathrm{pro}}+1}^{0} \left(S_{\mathrm{pro},i}^{+}\,S_{\mathrm{pro},-i'}^{-} + S_{\mathrm{pro},-i'}^{+}\,S_{\mathrm{pro},i}^{-}\right), \tag{3}$$

$$\hat{H}_{\mathrm{in}}^{\mathrm{n}} = \sum_{i=1}^{p_{\mathrm{n}}} \varepsilon_{i,\,\Omega_i}^{\mathrm{n}}\,\hat{n}_{i,\,\Omega_i}^{\mathrm{n}} - \sum_{i'=-p'_{\mathrm{n}}+1}^{0} \varepsilon_{-i',\,\Omega_{-i'}}^{\mathrm{n}}\,\hat{n}_{-i',\,\Omega_{-i'}}^{\mathrm{n}} + g_{\mathrm{n}} \sum_{i=1}^{p_{\mathrm{n}}} \sum_{i'=-p'_{\mathrm{n}}+1}^{0} \left(S_{\mathrm{n},i}^{+}\,S_{\mathrm{n},-i'}^{-} + S_{\mathrm{n},-i'}^{+}\,S_{\mathrm{n},i}^{-}\right), \tag{4}$$

where p_ρ and p'_ρ with $\rho = $ pro or n are the number of proton and neutron Nilsson levels above and at or below the Fermi surface of a given even-even nucleus considered, respectively. $\varepsilon_{j,\Omega_j}^{\rho}$ and $\varepsilon_{-i,\Omega_{-i}}^{\rho}$ are single-particle energies above and at or below the Fermi surface, respectively, which are generated from a Nilsson shell model code and rearranged with reference to the Fermi surface.

$$\hat{n}_{i,\Omega_i}^{\rho} = a_{\rho,i,\Omega_i}^{\dagger} a_{\rho,i,\Omega_i} + a_{\rho,i,\bar{\Omega}_i}^{\dagger} a_{\rho,i,\bar{\Omega}_i} \tag{5}$$

is the particle number operator of the i-th Nilsson level above the Fermi surface, and

$$\hat{n}_{-i',\Omega_{i'}}^{\rho} = a_{\rho,-i',-\Omega_{-i'}} a_{\rho,-i',-\Omega_{i'}}^{\dagger} + a_{\rho,-i,-\bar{\Omega}_{-i}} a_{\rho,-i,-\bar{\Omega}_{-i}}^{\dagger} \tag{6}$$

is the hole number operator of the $-i$-th Nilsson level at or below the Fermi surface, in which $a^{\dagger}_{\rho,i,\pm\Omega_i}$ ($a_{\rho,i,\pm\Omega_i}$) with $\rho =$ pro or n being the particle creation (annihilation) operator for the i-th Nilsson level with the quantum number Ω_i of the angular momentum projection to the z' axis of the intrinsic frame, while the operator with $\bar{\Omega}_i$ is the corresponding time-reversed one. The last term of (3) and (4) describes the interaction of the 2p- and 2h-pairs, which is assumed to be level-independent with real constant $g_{\rm pro} \approx g_{\rm n} = g < 0$ in the calculation, where

$$S^{+}_{\rho,i} = a^{\dagger}_{\rho,i\,\Omega_i}\, a^{\dagger}_{\rho,i\,\bar{\Omega}_i},\;\; S^{-}_{\rho,i} = (S^{+}_{\rho,i})^{\dagger},$$
$$S^{-}_{\rho,-i'} = a_{\rho,-i'\,-\Omega_{-i'}}\, a_{\rho,-i',-\bar{\Omega}_{-i'}},\;\; S^{+}_{\rho,-i'} = (S^{-}_{\rho,-i'})^{\dagger} \tag{7}$$

are $K = 0$ particle- and hole-pair creation and annihilation operators, respectively. As is well known, the RVM Hamiltonian is invariant under the intrinsic Vierergruppe (D_2) transformation. It is obvious that the D_2 symmetry is still preserved when the interactions among 2p- and 2h-pairs are involved. Since only one proton (neutron) particle-pair or hole-pair is considered, the proton (neutron) pairing interaction is neglected due to the fact that the pairing interaction of only one particle-pair or one hole-pair is relatively weak [36,37] in this case.

In the calculation, similar to the approximation made in the PRM with the RVM description of the core, rotational energies of the particles and holes, and the rotation-particle and rotation-hole coupling terms are also neglected [28]. An eigenstate of the RVM Hamiltonian (2) is written as $|n_\beta, n_\gamma, K, L\, M\rangle$, where n_β and n_γ are the number of β and γ phonons, respectively; L is the quantum number of the total angular momentum in this case; K and M are the quantum numbers of the angular momentum projected onto the z' axis of the intrinsic frame and z axis of the laboratory frame, respectively. The corresponding eigenvalue of (2) is given by [28]

$$E^{n_\beta,n_\gamma,K}_{L} = \tfrac{E_0}{2}\left(L(L+1) - K^2\right) + E_\gamma\left(\tfrac{K}{2} + 1 + 2n_\gamma\right) + E_\beta\,(n_\beta + \tfrac{1}{2}),$$
$$E_0 = \tfrac{\hbar^2}{\Im_0},\;\; E_\beta = \hbar\sqrt{\tfrac{C_0}{B}},\;\; E_\gamma = \hbar\sqrt{\tfrac{C_2}{B}}, \tag{8}$$

for $n_\beta = 0, 1, \cdots, n_\gamma = 0, 1, \cdots, K = 0, 2, 4, \cdots$, and for given K,

$$L = \begin{cases} K,\; K+1,\; \cdots, & \text{for } K \neq 0, \\ 0,\; 2,\; 4,\; \cdots, & \text{for } K = 0. \end{cases} \tag{9}$$

When there are p'_ρ (p_ρ) Nilsson levels below (above) the Fermi surface, eigenstates of the model Hamiltonian (1) in this case can be expressed as

$$|n_\beta, n_\gamma, K; \xi_{\rm pro}, \xi_{\rm n};\; L\, M\rangle = \mathcal{N}_{\xi_{\rm pro}}\mathcal{N}_{\xi_{\rm n}}\left(1 + \textstyle\sum_{i,j} C^{\xi_{\rm pro}}_{j,i}\, S^{+}_{{\rm pro},j} S^{-}_{{\rm pro},-i}\right) \times$$
$$\left(1 + \textstyle\sum_{i',j'} C^{\xi_{\rm n}}_{j',i'}\, S^{+}_{{\rm n},j'} S^{-}_{{\rm n},-i'}\right)|n_\beta, n_\gamma, K, L\, M\rangle, \tag{10}$$

where $|n_0, n_\gamma, K, L\, M\rangle$ is an eigenstate of the Hamiltonian of the core (2) and is assumed to be the vacuum state of particles outside of the core and the holes within the core, simultaneously; $C^{\xi_\rho}_{ji}$ is the expansion coefficient; and $\mathcal{N}_{\xi_\rho}$ is the normalization constant. In the following, except for the ground-state band with $\xi_{\rm pro} = \xi_{\rm n} = 1$, the other excited bands described by (10) are simply called 2p2h bands. In the calculation, the Fermi surface of protons or neutrons is determined by the last occupied Nilsson level of protons or neutrons at the ground state of the Nilsson shell model for a given even-even nucleus. Besides the eigenstates built on 0p0h shown in (10), there are those built on 1p1h excitation with a $K = 0$ 1p1h pair, which are the next lowest in energy to be considered with

$$|n_\beta, n_\gamma, K;\ (-i'_\rho, j'_\rho);\ \xi_{\rm pro}, \xi_{\rm n};\ L\,M\rangle = \mathcal{N}_{\xi_{\rm pro}}\mathcal{N}_{\xi_{\rm n}}\left(1+\sum\nolimits'_{i,j} C^{\xi_{\rm pro}}_{j,i}\, S^+_{{\rm pro},j} S^-_{{\rm pro},-i}\right)\left(1+\sum\nolimits'_{i'',j''} C^{\xi_{\rm n}}_{j'',i''}\, S^+_{{\rm n},j''} S^-_{{\rm n},-i''}\right)\times |(-i'_\rho, j'_\rho);\ n_\beta, n_\gamma, K, L\,M\rangle, \tag{11}$$

where the summation is over the Nilsson levels not occupied by the single-particle and the single-hole, namely, j'_ρ and $-i'_\rho$ levels are excluded within the sum, and

$$|(-i'_\rho, j'_\rho);\ n_\beta, n_\gamma, K, L\,M\rangle = S^+_{\rho, j'_\rho, -i'_\rho}|n_\beta,\ n_\gamma, K,\ L\,M\rangle \tag{12}$$

with [1]

$$S^+_{\rho, j'_\rho, -i'_\rho} = \sqrt{\frac{1}{2}}\left(a^\dagger_{\rho, j'_\rho, \Omega_{j'_\rho}} a_{\rho, -i'_\rho, -\bar{\Omega}_{-i'_\rho}} - a^\dagger_{\rho, j'_\rho, \bar{\Omega}_{j'_\rho}} a_{\rho, -i'_\rho, -\Omega_{-i'_\rho}}\right), \tag{13}$$

in which j'_ρ and $-i'_\rho$ stand for the Nilsson levels occupied by the single particle and hole with the same parity, satisfying $\Omega_{j'_\rho} = \Omega_{-i'_\rho}$. The excitation bands described by (11) are called 1p1h bands.

The expansion coefficients in (10) and (11) can be expressed as

$$C^{\xi_\rho}_{ji} = \frac{g}{E^{\xi_\rho} + 2\epsilon^\rho_{-i_\rho,\ \Omega_{-i_\rho}} - 2\epsilon^\rho_{j_\rho,\ \Omega_{j_\rho}}}, \tag{14}$$

where E^{ξ_ρ} should satisfy

$$E^{\xi_\rho} = \sum\nolimits'_{i,j} \frac{g^2}{E^{\xi_\rho} + 2\epsilon^\rho_{-i_\rho,\ \Omega_{-i_\rho}} - 2\epsilon^\rho_{j_\rho,\ \Omega_{j_\rho}}}, \tag{15}$$

in which ξ_ρ stands for the ξ_ρ-th root of (15), while the prime stands for the exclusion of occupied Nilsson level. The eigenvalues of (1) corresponding to the eigenstates (10) are given by

$$E^{n_\beta, n_\gamma, K}_{\xi_\pi, \xi_\nu, LM} = E^{n_\beta, n_\gamma, K}_L + E^{\xi_\pi} + E^{\xi_\nu}, \tag{16}$$

while those corresponding to the eigenstates (11) are given by

$$E^{(-i'_\rho, j'_\rho); n_\beta, n_\gamma, K}_{\xi_\pi, \xi_\nu, LM} = E^{n_\beta, n_\gamma, K}_L + E^{\xi_\pi} + E^{\xi_\nu} - \epsilon^\rho_{-i'_\rho,\ \Omega_{-i'_\rho}} + \epsilon^\rho_{j'_\rho,\ \Omega_{j'_\rho}}. \tag{17}$$

Similar to the multi-particle-hole configuration mixing schemes in the interacting boson model [38–40], the E2 operator is defined as

$$T_\mu({\rm E2}) = Q^{\rm c}_\mu + Q^{\rm ph}_\mu + \sum\nolimits_\rho \lambda_\rho P_\rho\left(Q^{\rm c}_\mu + Q^{\rm ph}_\mu\right)P_\rho + \lambda_{\rm pro,n} P_{\rm pro} P_{\rm n}\left(Q^{\rm c}_\mu + Q^{\rm ph}_\mu\right)P_{\rm n} P_{\rm pro}, \tag{18}$$

where P_ρ is the projection operator, which projects onto the 0p0h, 2p2h and 1p1h, 3p3h even parity $K = 0$ subspace of protons or neutrons; $\lambda_{\rm pro}$, $\lambda_{\rm n}$, and $\lambda_{\rm pro,n}$ are the configuration mixing parameters; $Q^{\rm c}_\mu$ is the quadrupole operator of the RVM [25,28],

$$Q^{\rm c}_\mu = \frac{3ZeR_0^2}{4\pi}\left\{ D^{2*}_{\mu 0}(\theta)\left(\beta_0(1+\alpha) + \xi(1+2\alpha) + \alpha(\xi^2 - 2\eta^2)\right) + \left(D^{2*}_{\mu 2}(\theta) + D^{2*}_{\mu -2}(\theta)\right)\left((1-2\alpha)\eta - 2\alpha\xi\eta\right)\right\} \tag{19}$$

with $R_0 = 1.2\,\mathrm{A}^{1/3}$ fm for the nucleus with the mass number A and $\alpha = \sqrt{20/(7\pi)}\,\beta_0$, while $D^{2*}_{\mu\nu}(\theta)$ is the Wigner D-function of the Euler angles $\theta \equiv (\theta_1, \theta_2, \theta_3)$ and Q^{ph}_{μ} is the quadrupole operator of the particles and holes.

Since 1p1h bands are relatively high, if the 1p1h states (11) are not considered, only the diagonal part of Q^{ph}_{μ} contributes, which can be expressed as

$$Q^{\mathrm{ph,dig}}_{\mu} = D^{2*}_{\mu 0}(\theta) \sum_{\rho} \left(\sum_i q^{\rho}_i n^{\rho}_i + \sum_i \bar{q}^{\rho}_{-i} n^{\rho,\mathrm{h}}_{-i} \right) \tag{20}$$

with

$$\begin{aligned} q^{\rho}_i &= e_\rho\, r_0^2 \sum_{l,j,l',j'} W^i_{l'j'\Omega} W^i_{lj\Omega} \langle N_{\mathrm{o}}(l'\,\tfrac{1}{2})j'\Omega | (r/r_0)^2 Y_{20} | N_{\mathrm{o}}(l\,\tfrac{1}{2})j\Omega \rangle, \\ \bar{q}^{\rho}_{-i} &= -e_\rho\, r_0^2 \sum_{l,j,l',j'} W^{-i}_{l'j'\Omega} W^{-i}_{lj\Omega} \langle N_{\mathrm{o}}(l'\,\tfrac{1}{2})j'\Omega | (r/r_0)^2 Y_{20} | N_{\mathrm{o}}(l\,\tfrac{1}{2})j\Omega \rangle, \end{aligned} \tag{21}$$

where N_{o} is the number of phonons of a major oscillator shell; $r_0^2 = 1.012\,\mathrm{A}^{1/3}\,\mathrm{fm}^2$; e_ρ is the effective charge of the particles, of which the hole is taken to be the same absolute value of that of the particle but with the opposite sign; $W^i_{lj\Omega}$ is the expansion coefficients of the i-th Nilsson level in terms of the eigenstates of the spherical harmonic oscillator; $n^{\rho,\mathrm{h}}_{-i}$ is the number of holes in the Nilsson level $-i$; $(lj)j'$ stands for the angular momentum coupling; and the matrix element $\langle N_{\mathrm{o}}(l'\,\frac{1}{2})j'\Omega | (r/r_0)^2 Y_{20} | N_{\mathrm{o}}(l\,\frac{1}{2})j\Omega \rangle$ is given by

$$\begin{aligned} \langle N_{\mathrm{o}}(l'\,\tfrac{1}{2})j'\Omega | (r/r_0)^2 Y_{20} | N_{\mathrm{o}}(l\,\tfrac{1}{2})j\Omega \rangle = \sum_{l'' m_l m_s} \sqrt{\frac{5(2l+1)}{4\pi(2l''+1)}} \langle l' m_l; \tfrac{1}{2} m_s | j'\Omega \rangle \times \\ \langle l m_l; \tfrac{1}{2} m_s | j\Omega \rangle \langle l m_l; 2\,0 | l'' m_l \rangle \langle l0; 2\,0 | l''0 \rangle \langle N_{\mathrm{o}} l' | (r/r_0)^2 | N_{\mathrm{o}} l'' \rangle, \end{aligned} \tag{22}$$

where $\langle l m_l; \frac{1}{2} m_s | j\Omega \rangle$ etc. are the SU(2) Clebsch–Gordan (CG) coefficients, and

$$\begin{aligned} \langle N_{\mathrm{o}} l' | (r/r_0)^2 | N_{\mathrm{o}} l'' \rangle = (N_{\mathrm{o}} + \tfrac{3}{2}) \delta_{l'\,l''} + \\ \sqrt{(N_{\mathrm{o}} + l' + 1)(N - l' + 2)}\, \delta_{l''\,l'-2} + \sqrt{(N_{\mathrm{o}} + l' + 3)(N - l')}\, \delta_{l''\,l'+2}. \end{aligned} \tag{23}$$

The matrix element of the quadruple operator related to the eigenstates (10) is given by

$$\begin{aligned} \langle n_\beta, n_\gamma, K; \xi_{\mathrm{pro}}, \xi_{\mathrm{n}};\ L || T(\mathrm{E2}) || n'_\beta, n'_\gamma, K'; \xi'_{\mathrm{pro}}, \xi'_{\mathrm{n}};\ L' \rangle = \langle n_\beta, n_\gamma, K;\ L || Q^{\mathrm{c}} || n'_\beta, n'_\gamma, K';\ L' \rangle \times \\ \Big(\delta_{\xi'_{\mathrm{pro}}\xi_{\mathrm{pro}}} \delta_{\xi'_{\mathrm{n}}\xi_{\mathrm{n}}} (1 + \lambda_{\mathrm{pro}} + \lambda_{\mathrm{n}}) - \lambda_{\mathrm{pro}}\, \delta_{\xi'_{\mathrm{n}}\xi_{\mathrm{n}}} \mathcal{N}_{\xi'_{\mathrm{pro}}} \mathcal{N}_{\xi_{\mathrm{pro}}} - \lambda_{\mathrm{n}}\, \delta_{\xi'_{\mathrm{pro}}\xi_{\mathrm{pro}}} \mathcal{N}_{\xi'_{\mathrm{n}}} \mathcal{N}_{\xi_{\mathrm{n}}} + \\ \lambda_{\mathrm{pro,n}} (\delta_{\xi'_{\mathrm{pro}}\xi_{\mathrm{pro}}} - \mathcal{N}_{\xi'_{\mathrm{pro}}} \mathcal{N}_{\xi_{\mathrm{pro}}}) (\delta_{\xi'_{\mathrm{n}}\xi_{\mathrm{n}}} - \mathcal{N}_{\xi'_{\mathrm{n}}} \mathcal{N}_{\xi_{\mathrm{n}}}) \Big) + \\ \delta_{n'_\beta n_\beta} \delta_{n'_\gamma n_\gamma} \delta_{K'K} \textstyle\sum_\rho \Big(\delta_{\xi'_\rho \xi_\rho} (1 + \lambda_{\mathrm{pro}} + \lambda_{\mathrm{n}}) - \lambda_\rho\, \mathcal{N}_{\xi_\rho} \mathcal{N}_{\xi'_\rho} + \lambda_{\mathrm{pro,n}} (\delta_{\xi'_{\bar\rho}\xi_{\bar\rho}} - \mathcal{N}_{\xi_{\bar\rho}} \mathcal{N}_{\xi'_{\bar\rho}}) \Big) \Lambda^{\xi'_\rho \xi_\rho}_{L'LK}, \end{aligned} \tag{24}$$

in which $\langle n_\beta, n_\gamma, K;\ L || Q^{\mathrm{c}} || n'_\beta, n'_\gamma, K';\ L' \rangle$ is the reduced matrix element of the core part [28], where $\overline{\mathrm{pro}} = \mathrm{n}$, $\bar{\mathrm{n}} = \mathrm{pro}$, and

$$\Lambda^{\xi'_\rho \xi_\rho}_{L'LK} = 2 \langle L'\,K; 2\,0 | L\,K \rangle\, \mathcal{N}_{\xi'_\rho} \mathcal{N}_{\xi_\rho} \sum_{ji} C^{\xi'_\rho}_{j,i} C^{\xi_\rho}_{j,i} (q^\rho_j + \bar{q}^\rho_{-i}). \tag{25}$$

Thus, B(E2) values are given by [28]

$$B(\mathrm{E2};\, n_\beta, n_\gamma, K; \xi_{\mathrm{pro}}, \xi_{\mathrm{n}};\, L \to n'_\beta, n'_\gamma, K'; \xi'_{\mathrm{pro}}, \xi'_{\mathrm{n}};\, L') = \frac{2L'+1}{2L+1}\, |\langle n_\beta, n_\gamma, K; \xi_{\mathrm{pro}}, \xi_{\mathrm{n}};\, L||T(\mathrm{E2})||n'_\beta, n'_\gamma, K'; \xi'_{\mathrm{pro}}, \xi'_{\mathrm{n}};\, L'\rangle|^2. \tag{26}$$

The M1 operator is defined similarly as

$$T_\mu(\mathrm{M1}) = T_\mu^{\mathrm{RVM}}(\mathrm{M1}) + \textstyle\sum_\rho \lambda_\rho P_\rho \Big(T_\mu^{\mathrm{RVM}}(\mathrm{M1}) + T_\mu^{\mathrm{ph}}(\mathrm{M1})\Big) P_\rho + \lambda_{\mathrm{pro,n}} P_{\mathrm{pro}} P_{\mathrm{n}} \Big(T_\mu^{\mathrm{RVM}}(\mathrm{M1}) + T_\mu^{\mathrm{ph}}(\mathrm{M1})\Big) P_{\mathrm{n}} P_{\mathrm{pro}}, \tag{27}$$

where the same projection operators and configuration mixing parameters as those of the E2 operator (18) are used; $T_\mu^{\mathrm{RVM}}(\mathrm{M1})$ and $T_\mu^{\mathrm{ph}}(\mathrm{M1})$ are the M1 operator of the core described by the RVM and that of the particles and holes, respectively. The RVM core part is defined as

$$T_\mu^{\mathrm{RVM}}(\mathrm{M1}) = \sqrt{\tfrac{3}{4\pi}}\left(g_0 \hat{L}_\mu + \textstyle\sum_{i=1}^3 g_i (Q^{\mathrm{c}}(i) \times \hat{L})_\mu^{(1)}\right) \tag{28}$$

with four effective gyromagnetic ratios g_i ($i = 0, \cdots, 3$), where $\hat{L}_\mu$ are the angular momentum operators of the core in the laboratory frame, and

$$(Q^{\mathrm{c}}(i) \times \hat{L})_\mu^{(1)} = \sum_{\mu_1 \mu_2} \langle 2\mu_1; 1\mu_2 | 1\mu \rangle Q^{\mathrm{c}}_{\mu_1}(i) \hat{L}_{\mu_2} \tag{29}$$

with

$$Q^{\mathrm{c}}_\mu(1) = D^{2*}_{\mu 0}(\theta)(1+\alpha), \tag{30}$$

$$Q^{\mathrm{c}}_\mu(2) = D^{2*}_{\mu 0}(\theta)\Big((\xi/\beta_0)(1+2\alpha) + (\alpha/\beta_0)(\xi^2 - 2\eta^2)\Big), \tag{31}$$

$$Q^{\mathrm{c}}_\mu(3) = \left(D^{2*}_{\mu 2}(\theta) + D^{2*}_{\mu -2}(\theta)\right)\Big((1-2\alpha)(\eta/\beta_0) - 2(\alpha/\beta_0)\xi\eta\Big). \tag{32}$$

It is noted that the high-order terms involved in (28) are quite similar to those introduced in the IBM calculation with no distinction between protons and neutrons [41]. $T_\mu^{\mathrm{ph}}(\mathrm{M1})$ without high-order terms can be expressed as

$$T_\mu^{\mathrm{ph}}(\mathrm{M1}) = \sqrt{\frac{3}{4\pi}} \sum_{\mu'} D^{1*}_{\mu\mu'}(\theta) \sum_\rho \left(g_{\mathrm{p}}^\rho \hat{L}_{\mu'}^{\rho,\,\mathrm{p}} + g_{\mathrm{h}}^\rho \hat{L}_{\mu'}^{\rho,\,\mathrm{h}}\right), \tag{33}$$

where $\hat{L}_\mu^{\rho,\,\mathrm{p}}$ ($\hat{L}_\mu^{\rho,\,\mathrm{h}}$) is the angular momentum operator of the proton or neutron type particles (holes) in the intrinsic frame, and g_{p}^ρ (g_{h}^ρ) is the effective gyromagnetic ratio of neutron or proton type particle (hole). If the 1p1h states (11) are not considered, there is no contribution of (33) to the matrix element of (27) related to the eigenstates (10) due to the fact that the particles (holes) are paired with $K = 0$.

Hence, the matrix element of the M1 operator related to the eigenstates (10) is given by

$$\begin{aligned}
&\langle n'_\beta, n'_\gamma, K'; \xi'_{\mathrm{pro}}, \xi'_{\mathrm{n}};\, L'||T(\mathrm{M1})||n_\beta, n_\gamma, K; \xi_{\mathrm{pro}}, \xi_{\mathrm{n}};\, L\rangle = \langle n'_\beta, n'_\gamma, K';\, L'||T^{\mathrm{RVM}}(\mathrm{M1})||n_\beta, n_\gamma, K;\, L\rangle \times \\
&\Big(\delta_{\xi'_{\mathrm{pro}}\xi_{\mathrm{pro}}} \delta_{\xi'_{\mathrm{n}}\xi_{\mathrm{n}}}(1 + \lambda_{\mathrm{pro}} + \lambda_{\mathrm{n}}) - \lambda_{\mathrm{pro}}\, \delta_{\xi'_{\mathrm{n}}\xi_{\mathrm{n}}} \mathcal{N}_{\xi'_{\mathrm{pro}}} \mathcal{N}_{\xi_{\mathrm{pro}}} - \lambda_{\mathrm{n}}\, \delta_{\xi'_{\mathrm{pro}}\xi_{\mathrm{pro}}} \mathcal{N}_{\xi'_{\mathrm{n}}} \mathcal{N}_{\xi_{\mathrm{n}}} + \\
&\lambda_{\mathrm{pro,n}} (\delta_{\xi'_{\mathrm{pro}}\xi_{\mathrm{pro}}} - \mathcal{N}_{\xi'_{\mathrm{pro}}} \mathcal{N}_{\xi_{\mathrm{pro}}})(\delta_{\xi'_{\mathrm{n}}\xi_{\mathrm{n}}} - \mathcal{N}_{\xi'_{\mathrm{n}}} \mathcal{N}_{\xi_{\mathrm{n}}})\Big),
\end{aligned} \tag{34}$$

in which $\langle n'_\beta, n'_\gamma, K';\ L'||T^{\rm RVM}({\rm M1})||n_\beta, n_\gamma, K;\ L\rangle$ can be expressed as

$$\begin{aligned}\langle n'_\beta, n'_\gamma, K';\ L'||T^{\rm RVM}({\rm M1})||n_\beta, n_\gamma, K;\ L\rangle = g_0\sqrt{\frac{3L(L+1)}{4\pi}}\delta_{n'_\beta n_\beta}\delta_{n'_\gamma n_\gamma}\delta_{KK'}\delta_{LL'} + \\ (-1)^{L+L'+1}\sqrt{\frac{9L(L+1)(2L+1)}{4\pi}}\begin{Bmatrix} L' & 2 & L \\ 1 & L & 1 \end{Bmatrix}\sum_{i=1}^{3} g_i\langle n_\beta, n_\gamma, K;\ L||Q^{\rm c}(i)||n'_\beta, n'_\gamma, K';\ L'\rangle,\end{aligned} \tag{35}$$

where the 6j-symbol with six angular momentum quantum numbers in the braces is involved and explicit expressions of the reduced matrix elements $\langle n_\beta, n_\gamma, K;\ L||Q^{\rm c}(i)||n'_\beta, n'_\gamma, K';\ L'\rangle$ are provided in [28].

Thus, the magnetic dipole moment of a given state is defined by

$$\mu(n_\beta, n_\gamma, K; \xi_{\rm pro}, \xi_{\rm n}; L) = \sqrt{\tfrac{4\pi}{3}}\langle LL;\ 10|LL\rangle\langle n_\beta, n_\gamma, K; \xi_{\rm pro}, \xi_{\rm n};\ L||T({\rm M1})||n_\beta, n_\gamma, K; \xi_{\rm pro}, \xi_{\rm n};\ L\rangle. \tag{36}$$

B(M1) values are given by

$${\rm B}({\rm M1}; n_\beta, n_\gamma, K; \xi_{\rm pro}, \xi_{\rm n};\ L \to n'_\beta, n'_\gamma, K';\ L') = \frac{2L'+1}{2L+1}|\langle n'_\beta, n'_\gamma, K'; \xi'_{\rm pro}, \xi'_{\rm n};\ L'||T({\rm M1})||n_\beta, n_\gamma, K; \xi_{\rm pro}, \xi_{\rm n};\ L\rangle|^2. \tag{37}$$

Since only a few magnetic dipole moments of low-lying states and B(M1) values of the transitions between low-lying states in ^{154}Gd are experimentally available [29,42], E2/M1 mixing ratios defined in [41] with

$$\begin{aligned}\Delta(n_\beta, n_\gamma, K; \xi_{\rm pro}, \xi_{\rm n};\ L \to n'_\beta, n'_\gamma, K'; \xi'_{\rm pro}, \xi'_{\rm n};\ L') \equiv \\ \langle n_\beta, n_\gamma, K; \xi_{\rm pro}, \xi_{\rm n};\ L||T({\rm E2})||n'_\beta, n'_\gamma, K'; \xi'_{\rm pro}, \xi'_{\rm n};\ L'\rangle / \langle n'_\beta, n'_\gamma, K'; \xi'_{\rm pro}, \xi'_{\rm n};\ L'||T({\rm M1})||n_\beta, n_\gamma, K; \xi_{\rm pro}, \xi_{\rm n};\ L\rangle\end{aligned} \tag{38}$$

are calculated.

Similar to the E2 and M1 operators, if the 1p1h states (11) are not considered, the $E0$ operator can be effectively expressed as

$$\begin{aligned}T({\rm E0}) = T^{\rm c}(E0) + \textstyle\sum_\rho\sum_i(\Lambda^\rho_i n_i + \bar\Lambda^\rho_{-i}n^{\rho,{\rm h}}_{-i}) + \\ \textstyle\sum_\rho \lambda_\rho P_\rho\Big(T^{\rm c}(E0) + \sum_\rho\sum_i(\Lambda^\rho_i n_i + \bar\Lambda^\rho_{-i}n^{\rho,{\rm h}}_{-i})\Big)P_\rho + \quad (39) \\ \lambda_{\rm pro,n}P_{\rm pro}P_{\rm n}\Big(T^{\rm c}(E0) + \textstyle\sum_\rho\sum_i(\Lambda^\rho_i n_i + \bar\Lambda^\rho_{-i}n^{\rho,{\rm h}}_{-i})\Big)P_{\rm n}P_{\rm pro}, \quad (40)\end{aligned}$$

where the projection parameters λ_ρ and $\lambda_{\rm pro,n}$ are the same as those used in the E2 operator, the collective core part is given by [25,43]

$$T^{\rm c}(E0) = \tfrac{3ZeR_0^2}{4\pi}(\beta_0^2 + 2\beta_0\,\xi + \xi^2 + 2\eta^2), \tag{41}$$

$$\begin{aligned}\Lambda^\rho_i = e_\rho\, r_0^2\sum_{l,j,l',j'} W^i_{l'j'\Omega}W^i_{lj\Omega}\langle N_{\rm o}(l'\,\frac{1}{2})j'\Omega|(r/r_0)^2|N_{\rm o}(l\,\frac{1}{2})j\Omega\rangle, \\ \bar\Lambda^\rho_{-i} = -e_\rho\, r_0^2\sum_{l,j,l',j'} W^{-i}_{l'j'\Omega}W^{-i}_{lj\Omega}\langle N_{\rm o}(l'\,\frac{1}{2})j'\Omega|(r/r_0)^2|N_{\rm o}(l\,\frac{1}{2})j\Omega\rangle.\end{aligned} \tag{42}$$

Similar to (22), the matrix element $\langle N_{\rm o}(l'\,\frac{1}{2})j'\Omega|(r/r_0)^2|N_{\rm o}(l\,\frac{1}{2})j\Omega\rangle$ is given by

$$\begin{aligned}\langle N_{\rm o}(l'\,\tfrac{1}{2})j'\Omega|(r/r_0)^2|N_{\rm o}(l\,\tfrac{1}{2})j\Omega\rangle = \textstyle\sum_{m_l m_s}\langle l'm_l;\,\tfrac{1}{2}m_s|j'\Omega\rangle\times \\ \langle lm_l;\,\tfrac{1}{2}m_s|j\Omega\rangle\langle N_{\rm o}l'|(r/r_0)^2|N_{\rm o}l\rangle.\end{aligned} \tag{43}$$

The matrix element of the E0 operator related to the eigenstates (10) is given by

$$
\begin{aligned}
&\langle n'_\beta, n'_\gamma, K'; \xi'_{\rm pro}, \xi'_{\rm n};\; L' || T({\rm E0}) || n_\beta, n_\gamma, K; \xi_{\rm pro}, \xi_{\rm n};\; L\rangle \\
&= \delta_{L'L}\, \langle n'_\beta, n'_\gamma, K';\, L || T^{\rm c}(E0) || n_\beta, n_\gamma, K;\, L\rangle \times \\
&\Big(\delta_{\xi'_{\rm pro}\xi_{\rm pro}}\delta_{\xi'_{\rm n}\xi_{\rm n}}(1+\lambda_{\rm pro}+\lambda_{\rm n}) - \lambda_{\rm pro}\,\delta_{\xi'_{\rm n}\xi_{\rm n}}\mathcal{N}_{\xi'_{\rm pro}}\mathcal{N}_{\xi_{\rm pro}} - \lambda_{\rm n}\,\delta_{\xi'_{\rm pro}\xi_{\rm pro}}\mathcal{N}_{\xi'_{\rm n}}\mathcal{N}_{\xi_{\rm n}} + \\
&\lambda_{\rm pro,n}(\delta_{\xi'_{\rm pro}\xi_{\rm pro}} - \mathcal{N}_{\xi'_{\rm pro}}\mathcal{N}_{\xi_{\rm pro}})(\delta_{\xi'_{\rm n}\xi_{\rm n}} - \mathcal{N}_{\xi'_{\rm n}}\mathcal{N}_{\xi_{\rm n}})\Big) + \\
&\delta_{n'_\beta n_\beta}\delta_{n'_\gamma n_\gamma}\delta_{K'K}\delta_{L'L}\sum_\rho \Big(\delta_{\xi'_\rho\xi_\rho}(1+\lambda_{\rm pro}+\lambda_{\rm n}) - \lambda_\rho\,\mathcal{N}_{\xi_\rho}\mathcal{N}_{\xi'_\rho} + \lambda_{\rm pro,n}(\delta_{\xi'_{\bar\rho}\xi_{\bar\rho}} - \mathcal{N}_{\xi_{\bar\rho}}\mathcal{N}_{\xi'_{\bar\rho}})\Big)\Lambda^{\xi'_\rho\xi_\rho},
\end{aligned}
\tag{44}
$$

where

$$
\Lambda^{\xi'_\rho\xi_\rho} = 2\,\mathcal{N}_{\xi'_\rho}\mathcal{N}_{\xi_\rho}\sum_{ji} C^{\xi'_\rho}_{j,i} C^{\xi_\rho}_{j,i}(\Lambda^\rho_j + \bar\Lambda^\rho_{-i}).
\tag{45}
$$

Accordingly, B(E0) and ρ^2(E0) values are given by [25,43]

$$
\begin{aligned}
&B({\rm E0};\, n_\beta, n_\gamma, K; \xi_\pi, \xi_\nu;\, L \to n'_\beta, n'_\gamma, K'; \xi'_\pi, \xi'_\nu;\, L) = \\
&|\langle n'_\beta, n'_\gamma, K'; \xi'_\pi, \xi'_\nu;\, L || T({\rm E0}) || n_\beta, n_\gamma, K; \xi_\pi, \xi_\nu;\, L\rangle|^2
\end{aligned}
\tag{46}
$$

and

$$
\begin{aligned}
&\rho^2({\rm E0};\, n_\beta, n_\gamma, K; \xi_\pi, \xi_\nu;\, L \to n'_\beta, n'_\gamma, K'; \xi'_\pi, \xi'_\nu;\, L) = \\
&\frac{1}{e^2 R_0^4} B({\rm E0};\, n_\beta, n_\gamma, K; \xi_\pi, \xi_\nu;\, L \to n'_\beta, n'_\gamma, K'; \xi'_\pi, \xi'_\nu;\, L).
\end{aligned}
\tag{47}
$$

3. Model Fit to ^{154}Gd

Low-lying bands of ^{154}Gd have been studied theoretically using the dynamic deformation model [15], the coherent state model [16], and the interacting boson model [17–23]. However, only the ground-state, beta-, and gamma-bands were discussed. In this section, we take ^{154}Gd as an example to be fitted by the present model. The deformation parameters $\epsilon_2 = 0.22$ corresponding to $\beta_0 \approx 0.232$ and $\epsilon_4 = -0.04$ for the Nilsson single-particle energies of ^{154}Gd are taken from [44], with which a few Nilsson single-particle energies of protons and neutrons near the Fermi surface corresponding to proton number Z = 64 and neutron number N = 90 are shown in Table 1. The lowest four pure 1p1h excitation energies with two of neutrons and two of protons are also shown in the lower part of Table 1.

Table 1. The neutron and proton single-particle energies (in MeV) of ^{154}Gd generated from the Nilsson model with $\epsilon_2 = 0.22$ and $\epsilon_4 = -0.04$, in which the parity of the levels is also shown.

Neutron	$\varepsilon^{\rm n(+)}_{-4,3/2}$	$\varepsilon^{\rm n(-)}_{-3,1/2}$	$\varepsilon^{\rm n(-)}_{-2,11/2}$	$\varepsilon^{\rm n(-)}_{-1,3/2}$	$\varepsilon^{\rm n(+)}_{0,1/2}$	$\varepsilon^{\rm n(+)}_{1,3/2}$	$\varepsilon^{\rm n(-)}_{2,3/2}$	$\varepsilon^{\rm n(-)}_{3,5/2}$	$\varepsilon^{\rm n(+)}_{4,5/2}$	$\varepsilon^{\rm n(-)}_{5,1/2}$	$\varepsilon^{\rm n(-)}_{6,5/2}$
	−1.532	−0.628	−0.607	−0.244	0	0.821	1.127	1.706	2.043	2.790	2.856
Proton	$\varepsilon^{\rm pro(-)}_{-5,1/2}$	$\varepsilon^{\rm pro(+)}_{-4,3/2}$	$\varepsilon^{\rm pro(+)}_{-3,1/2}$	$\varepsilon^{\rm pro(-)}_{-2,3/2}$	$\varepsilon^{\rm pro(+)}_{-1,5/2}$	$\varepsilon^{\rm pro(-)}_{0,5/2}$	$\varepsilon^{\rm pro(+)}_{1,3/2}$	$\varepsilon^{\rm pro(-)}_{2,7/2}$	$\varepsilon^{\rm pro(+)}_{3,7/2}$	$\varepsilon^{\rm pro(+)}_{4,1/2}$	$\varepsilon^{\rm pro(+)}_{5,5/2}$
	−1.740	−1.672	−1.629	−1.068	−0.016	0	0.187	1.236	1.280	1.608	1.663

Neutron-1h1p: $-\varepsilon^{\rm n(+)}_{-4,3/2} + \varepsilon^{\rm n(+)}_{1,3/2} = 2.353$, $-\varepsilon^{\rm n(-)}_{-1,3/2} + \varepsilon^{\rm n(-)}_{2,3/2} = 1.370$. Proton-1h1p: $-\varepsilon^{\rm pro(+)}_{-4,3/2} + \varepsilon^{\rm pro(+)}_{1,3/2} = 1.859$, $-\varepsilon^{\rm pro(+)}_{-1,5/2} + \varepsilon^{\rm pro(+)}_{5,5/2} = 1.679$.

We use the model Hamiltonian (1) to fit positive parity level energies below 1.990 MeV in the eight experimentally identified positive parity bands of ^{154}Gd provided in the level scheme of [29], while the level energy of 5^+_3 state is taken from the recent thesis [45]. In the fitting, 20 Nilsson single-particle energies of both protons and neutrons near the Fermi surface are taken with $p_\rho = p'_\rho = 10$. It is observed that the level energies (in MeV) only vary at the second decimal place if more Nillson single-particle energies are taken into account when $|g| \leq 0.3$ MeV, and can be readjusted by the interaction strength g. The calculation shows that the more the Nillson levels are taken into account, the smaller the interaction strength $|g|$ required in order to obtain a best fit to the 0^+ band head energies concerned. Therefore, the actual interaction strength $|g|$ is smaller than that shown in Table 2. The first part of Table 2 shows the fitting results of level energies below 1.990 MeV in the eight experimentally identified positive parity bands provided in [29,45], where the band numbers are assigned in [29], and the underlined 4_7^+ and 4_8^+ level energies above 1.990 MeV in bands 11 and 12, respectively, are also shown. It should be noted that spin and parity of the level energy at 2.088 MeV assigned to be 4_8^+ in this work are not determined in experiments [29]. In the fitting, it is observed that the gap of the first and the second 2p2h excitation energies is always less than 0.3 MeV if the interaction strength $|g| \leq 0.3$ MeV is considered. As the consequence, the first two 2p2h excitations may be the 0_3^+ and 0_4^+ band heads or the 0_4^+ and 0_5^+ band heads, of which the gaps are around 0.15 MeV. Accordingly, in Scheme 1 (S1), the 0_3^+ band head is fitted as the first 2p2h state. Hence, the beta-vibration energy E_β and the interaction strength g are adjusted according to the 0_2^+ and 0_3^+ excitation energies, respectively. In Scheme 2 (S2), the 0_4^+ band head is fitted as the first 2p2h state, for which the beta-vibration energy E_β is adjusted according to the 0_2^+ and 0_3^+ excitation energies, while the interaction strength g is adjusted according to the 0_4^+ excitation energy. The lower part of Table 2 provides the fitting results of a series of 0^+ excitation energies up to 0_{16}^+ in the two schemes, where $n\beta$ stands for $n_\beta = n$ and $K = 0$; $n\gamma$ stands for $n_\gamma = n$ and $K = 0$; 2p2h stands for the 2p2h-band head with $K = 0$, $n_\beta = 0$, $n_\gamma = 0$; and 1p1h stands for 1p1h-band head with $K = 0$, $n_\beta = 0$, $n_\gamma = 0$. The lowest eight 0^+ excitation energies obtained from the RVM are also provided. The fitting results of the levels in the eight bands in comparison to the experimental ones are shown in Figure 1.

Table 2. Level energies below 1.990 MeV in the eight experimentally identified positive parity bands of ^{154}Gd [29,45]. The parameters used in S1 (S2) for the ^{154}Gd core are $E_0 = 0.033$ (0.033) MeV, $E_\beta = 0.681$ (0.636) MeV, $E_\gamma = 0.780$ (0.780) MeV, and $g = -0.239$ (-0.2685) MeV.

	Band 1	(0_g^+ band)		Band 2	(0_2^+ band)			Band 4	(2_3^+ band)		Band 8	(2_5^+ band)	
L_ξ^+	Exp. [29]	S1 & S2	L_ξ^+	Exp. [29]	S1	S2	L_ξ^+	Exp. [29]	S1 & S2	L_ξ^+	Exp. [29]	S1	S2
2_1^+	0.123	0.100	0_2^+	0.681	0.681	0.636	2_3^+	0.996	0.813	2_5^+	1.531	1.494	1.449
4_1^+	0.371	0.333	2_2^+	0.815	0.781	0.736	3_1^+	1.128	0.913	3_2^+	1.661	1.594	1.549
6_1^+	0.718	0.700	4_2^+	1.048	1.014	0.969	4_3^+	1.264	1.047	4_6^+	1.789	1.728	1.683
8_1^+	1.144	1.200	6_2^+	1.366	1.381	1.336	5_1^+	1.432	1.213	5_3^+	1.990 [45]	1.894	1.849
10_1^+	1.637	1.833	8_2^+	1.756	1.881	1.836	6_3^+	1.607	1.413				
							7_1^+	1.810	1.647				

	Band 6	(0_3^+ band)			Band 10	(4_4^+ band)		Band 11	(0_6^+ band)			Band 12	(0_7^+ band)	
L_ξ^+	Exp. [29]	S1	S2	L_ξ^+	Exp. [29]	S1 & S2	L_ξ^+	Exp. [29]	S1	S2	L_ξ^+	Exp. [29]	S1	S2
0_3^+	1.182	1.182	1.272	4_4^+	1.646	1.626	0_6^+	1.574	1.551	1.560	0_7^+	1.650	1.560	1.587
2_4^+	1.418	1.282	1.372	5_2^+	1.770	1.793	2_6^+	1.716	1.651	1.660	2_7^+	1.775	1.660	1.687
4_5^+	1.701	1.515	1.605	6_4^+	1.912	1.993	4_7^+	$\underline{2.080}$	1.884	1.893	4_8^+	$\underline{2.088}$	1.893	1.920

	0_2^+	0_3^+	0_4^+	0_5^+	0_6^+	0_7^+	0_8^+	0_9^+	0_{10}^+	0_{11}^+	0_{12}^+	0_{13}^+	0_{14}^+	0_{15}^+	0_{16}^+
Exp. [29]	0.681	1.182	1.353	1.498	1.574	1.650	1.837	1.899	1.943	2.040	2.300	2.485	2.586	2.744	2.855
S1	0.681 β	1.182 2p2h	1.272 2p2h	1.362 2β	1.551 1p1h	1.560 γ	1.863 2p2h-β	1.870 1p1h	1.953 2p2h-β	2.043 3β	2.078 1p1h	2.232 1p1h-β	2.241 β-γ	2.399 2p2h	2.523 1p1h
S2	0.636 β	1.272 2β	1.353 2p2h	1.449 2p2h	1.560 γ	1.587 1p1h	1.905 1p1h	1.908 3β	1.989 2p2h-β	2.085 2p2h-β	2.113 1p1h	2.196 β-γ	2.223 1p1h-β	2.541 1p1h-β	2.544 4β
RVM	0.636 β	1.272 2β	1.560 γ	1.908 3β	2.196 β-γ	2.544 4β	2.832 2β-γ	3.120 2γ							

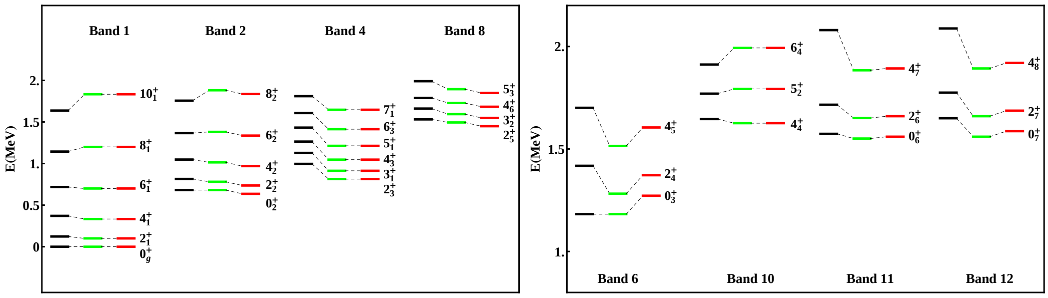

Figure 1. Low-lying level energies (in MeV) in the eight experimentally identified positive parity bands of ^{154}Gd, where the left (black) levels are those observed in experiments [29], the middle (green) levels are those obtained from Scheme 1, and the right (red) levels are those obtained from Scheme 2.

In the fitting to the level energies,

$$\sigma(E) = \left(\frac{1}{\mathcal{N}} \sum_{i=1}^{\mathcal{N}} (E_i^{\rm exp} - E_i^{\rm th})^2 \right)^{1/2} \tag{48}$$

is used, where $\mathcal{N}$ is the number of data used in the fitting, $E_i^{\rm th}$ is a level energy obtained from this work, and $E_i^{\rm exp}$ is the corresponding experimental value. As far as the level energies in the eight bands are concerned, $\sigma_{\rm S1}(E) = 0.113$ MeV and $\sigma_{\rm S2}(E) = 0.167$ MeV indicate that S1 is a little better than S2 in fitting to the level energies. The fitting quality of the RVM is the same as that of S2 if the level energies in bands 11 and 12 are excluded. As is clearly shown in the lower part of Table 2, the 0_u^+ ($u \geq 4$) band head energies produced from the RVM are much higher than the corresponding experimental results, while 0_u^+ ($u \leq 11$) level energies are well reproduced in both S1 and S2.

Table 3 shows the intra- and inter-band reduced E2 transition probabilities of the lowest three bands, namely, the ground-state band ($n_\beta = 0, K = 0, n_\gamma = 0$), the 0_2^+-band ($n_\beta = 1, K = 0, n_\gamma = 0$), and the gamma-band ($n_\beta = 0, K = 2, n_\gamma = 0$) calculated from S1, S2, and the RVM. The common feature of S1, S2, and the RVM results shown in Table 3 is that the B(E2) values of the intra-band transitions in the ground-state band are equal to the corresponding ones in the 0_2^+-band. The root mean square deviation of these B(E2) values is defined similar to that of the level energies shown in (48) is $\sigma_{\rm S1}(B(E2)) = 0.322$ e^{2}b^2 in S1, $\sigma_{\rm S2}(B(E2)) = 0.285$ e^{2}b^2 in S2, and $\sigma_{\rm RVM}(B(E2)) = 0.344$ e^{2}b^2 in the RVM. Hence, the RVM with particle-hole configuration mixing seems much better than the original RVM in describing the level energies and slightly better in the intra- and inter-band reduced E2 transition probabilities of the lowest three bands. Moreover, only the electric quadrupole moment of the 2_1^+ state of ^{154}Gd is experimentally available. $Q(2_1^+)$ calculated from S1, S2, and the RVM are -2.755 eb, -2.850 eb, and -2.688 eb, respectively, which are all a little larger than the experimental value $Q_{\rm exp}(2_1^+) = -1.82\,(4)$ eb [29]. Table 4 shows the branching ratios B(E2; $L_{\rm i}^+ \to L_{\rm f}'^+$)/B(E2; $L_{\rm i}^+ \to L_{\rm f}^+$). It can be observed that the B(E2) ratios of the transitions within the lowest three bands obtained from S1, S2, and the RVM shown on the left part of Table 4 are almost the same, among which most of the ratios are merely proportional to the square of the ratio of the related CG coefficients. Although there is discrepancy in comparison to the corresponding experimental values, the data pattern of these ratios follows that of the experimental data, which also indicate that most of these ratios are irrelevant to the particle-hole excitation. The most noticeable deviation occurs in the B(E2) ratios of the transitions from the 0_3^+ band to the beta-band and those from the 0_3^+ band to the ground-state band shown in the right part of Table 4. Most of these ratios obtained from S1 are too small, while they are too large in both S2 and the RVM. The fitting quality of the dynamic pairing plus quadrupole model [15,46] for these ratios [46] is quite similar to that of S2 or the RVM. As shown in Table 2, the 0_3^+ band head is assigned as the first 2p2h state, while it is the two β-phonon ($n_\beta = 2$) state in both S2 and the RVM.

A model calculation with a mixing of the two configurations determined in S1 and S2 may improve the results but there will be many parameters involved. The two exceptions are the ratios B(E2; $4_5^+ \to 2_4^+$)/B(E2; $4_5^+ \to 4_1^+$) and B(E2; $4_6^+ \to 4_2^+$)/B(E2; $4_6^+ \to 2_1^+$). The former is 84.0, 26.4, and 25.5 times larger in S1, S2, and the RVM, respectively, than the experimental value, while the latter is about 18 times larger in S1, S2, and the RVM than the experimental value.

Table 3. B(E2) values (in e^2b^2) of ^{154}Gd with the model parameters shown in Table 2 and the configuration mixing parameters $\lambda_{\rm pro} = -0.3305$, $\lambda_{\rm n} = 0.650$, $\lambda_{\rm pro,n} = 0.350$ and effective charge $e_{\rm pro} = 1.0\,e$, $e_{\rm n} = 0$ in S1, and $\lambda_{\rm pro} = 0.100$, $\lambda_{\rm n} = 0.40$, $\lambda_{\rm pro,n} = -0.80$, $e_{\rm pro} = 1.2\,e$, $e_{\rm n} = -0.2\,e$ in S2, where the symbol "–" indicates that the corresponding value is experimentally not available.

	Exp. [29]	S1	S2	RVM		Exp. [16,29]	S1	S2	RVM		Exp. [29]	S1	S2	RVM
$2_1^+ \to 0_g^+$	0.770	0.529	0.561	0.503	$2_2^+ \to 0_2^+$	0.476	0.529	0.561	0.503	$2_3^+ \to 0_2^+$	0.006	0.0001	0.0001	0.0001
$4_1^+ \to 2_1^+$	1.201	0.756	0.802	0.719	$4_2^+ \to 2_2^+$	1.220	0.756	0.802	0.719	$2_3^+ \to 4_1^+$	0.008	0.003	0.003	0.003
$6_1^+ \to 4_1^+$	1.398	0.832	0.883	0.791	$6_2^+ \to 4_2^+$	1.110	0.832	0.883	0.791	$2_3^+ \to 2_1^+$	0.060	0.057	0.060	0.055
$8_1^+ \to 6_1^+$	1.530	0.872	0.924	0.828	$8_2^+ \to 6_2^+$	–	0.872	0.924	0.828	$2_3^+ \to 0_g^+$	0.028	0.040	0.042	0.038
$10_1^+ \to 8_1^+$	1.765	0.895	1.024	0.851										
$0_2^+ \to 2_1^+$	0.255	0.193	0.218	0.198	$4_2^+ \to 6_1^+$	0.120	0.102	0.115	0.104					
$2_2^+ \to 4_1^+$	0.096	0.099	0.112	0.102	$4_2^+ \to 4_1^+$	0.038	0.058	0.066	0.059					
$2_2^+ \to 2_1^+$	0.033	0.055	0.062	0.056	$4_2^+ \to 2_1^+$	0.004	0.064	0.072	0.066					
$2_2^+ \to 0_g^+$	0.004	0.039	0.044	0.040	$6_2^+ \to 4_1^+$	0.003	0.057	0.079	0.072					

Table 4. The same as Table 3 but for the branching ratio $\frac{B(E2;L_i^+ \to L_f'^+)}{B(E2;L_i^+ \to L_f^+)}$.

	Exp.	S1	S2	RVM		Exp.	S1	S2	RVM
$\frac{6_2^+ \to 4_1^+}{6_2^+ \to 6_1^+}$	0.080 [16]; 0.043 [45]	1.236	1.236	1.236	$\frac{2_4^+ \to 0_2^+}{2_4^+ \to 0_g^+}$	4.6 [46]	0.950	2491.32	2491.32
$\frac{8_2^+ \to 6_1^+}{8_2^+ \to 6_2^+}$	0.006 [16]	0.085	0.090	0.091	$\frac{2_4^+ \to 4_2^+}{2_4^+ \to 2_2^+}$	1.531 [45], 0.79 [46]	1.800	1.800	1.800
$\frac{2_3^+ \to 2_2^+}{2_3^+ \to 2_1^+}$	1.000 [16]	0.003	0.003	0.003	$\frac{2_4^+ \to 0_2^+}{2_4^+ \to 2_2^+}$	0.027 [46]	0.700	0.700	0.700
$\frac{3_1^+ \to 2_1^+}{3_1^+ \to 4_1^+}$	1.006 [16]	2.500	2.500	2.500	$\frac{2_4^+ \to 2_2^+}{2_4^+ \to 2_1^+}$	100.000 [45], 79.2 [46]	0.950	2491.32	2491.32
$\frac{4_3^+ \to 2_1^+}{4_3^+ \to 4_1^+}$	0.148 [16], 0.125 [45]	0.340	0.340	0.340	$\frac{2_4^+ \to 4_2^+}{2_4^+ \to 4_1^+}$	10.000 [45], 5.6 [46]	0.950	2491.32	2491.32
$\frac{4_3^+ \to 6_1^+}{4_3^+ \to 4_1^+}$	0.270 [16], 0.264 [45]	0.086	0.086	0.086	$\frac{4_5^+ \to 4_2^+}{4_5^+ \to 4_1^+}$	74.118 [45], 45.5 [46]	0.950	2491.32	2491.32
$\frac{4_3^+ \to 2_3^+}{4_3^+ \to 4_1^+}$	8.251 [45]	4.476	4.476	4.476	$\frac{4_5^+ \to 2_2^+}{4_5^+ \to 4_1^+}$	3.235 [45]	1.044	2740.45	2740.45
$\frac{5_1 \to 3_1}{5_1 \to 6_1}$	18.051 [45]	13.844	13.844	13.844	$\frac{4_5 \to 2_4}{4_5 \to 4_1}$	588.235 [45]	49,404.8	15,506.1	15,027.5
$\frac{5_1^+ \to 4_1^+}{5_1^+ \to 6_1^+}$	0.744 [16], 0.585 [45]	1.750	1.750	1.750	$\frac{4_5^+ \to 6_1^+}{4_5^+ \to 4_1^+}$	10.294 [45]	1.750	1.750	1.750
$\frac{6_3^+ \to 4_1^+}{6_3^+ \to 6_1^+}$	0.081 [16], 0.096 [45]	0.269	0.269	0.269	$\frac{4_6^+ \to 4_1^+}{4_6^+ \to 2_1^+}$	7.778 [45]	2.945	2.945	2.945
$\frac{7_1^+ \to 8_1^+}{7_1^+ \to 6_1^+}$	2.532 [45]	0.667	0.667	0.667	$\frac{4_6^+ \to 4_2^+}{4_6^+ \to 2_1^+}$	55.556 [45]	1001.91	935.71	935.71
$\frac{2_4^+ \to 0_g^+}{2_4^+ \to 2_1^+}$	0.510 [45], 0.46 [46]	0.700	0.700	0.700	$\frac{5_3^+ \to 4_2^+}{5_3^+ \to 4_3^+}$	0.409 [45]	1.484	1.386	1.386
$\frac{2_4^+ \to 4_1^+}{2_4^+ \to 2_1^+}$	15.306 [45], 11.3 [46]	1.800	1.800	1.800					

However, there are only a few magnetic dipole moments of low-lying states, and B(M1) values of the transitions between low-lying states are experimentally available [42]. Therefore, experimentally deduced $\Delta \equiv$ E2/M1 ratios reported in [41] are calculated in order to validate the theory. In principle, the two experimentally measured magnetic dipole moments and two B(M1) values can be used to fix the four gyromagnetic ratios in (28). In the calculation, g_0, g_1, and g_2 are fixed by the two magnetic dipole moments and B(M1, $2_2^+ \to 2_1^+$), respectively, while g_3 is determined by a least square fit to the known E2/M1 ratios of the transitions from the 2_3^+ band to the ground-state band. The four gyromagnetic ratios thus determined, together with the two magnetic dipole moments and two B(M1) values, are shown in Table 5. It can be noticed in Table 5 that B(M1, $2_3^+ \to 2_1^+$) in S1, S2, and the RVM is about 2 times smaller than the experimental value in order to obtain a best fit to the E2/M1 ratios of the inter-band transitions from the 2_3^+ band to the ground-state band. The calculated results of the E2/M1 ratios in comparison to the experimental data [41] are shown in Table 6, in which the IBM results of these ratios [41] are also included for comparison. It is shown in Table 6 that the ratios of the inter-band transitions obtained from both S1 and S2 are the same, which is due to the fact that these ratios are independent of the configuration mixing parameters, while the only intra-band transition calculated in S1 is slightly different from that in S2, because the configuration mixing parameters and the contribution to the E2 matrix element from particles and holes are involved. The deviation from the experimental E2/M1 values defined similar to that of the level energies shown in (48) is $\sigma_{\text{S1,S2}}(\Delta) = 2.15$ eb$/\mu_N$, $\sigma_{\text{RVM}}(\Delta) = 2.17$ eb$/\mu_N$, and $\sigma_{\text{IBM}}(\Delta) = 4.04$ eb$/\mu_N$, in which $\Delta(3_1^+ \to 2_3^+)$ is excluded due to the uncertain experimental value. Therefore, except that the B(M1, $2_3^+ \to 2_1^+$) obtained from S1, S2, and the RVM is about two times smaller than the experimental value, which was not calculated in the IBM fit [41], the S1 and S2 results are the best.

Table 5. The effective gyromagnetic ratios g_i ($i = 0, \cdots, 3$) (in nuclear magneton μ_N) used in Scheme 1, Scheme 2, and the RVM, and the fitting results to the known magnetic moments (in μ_N) and B(M1) values (in Weisskopf unit) of ^{154}Gd.

	$\mu(2_1^+)$	$\mu(2_3^+)$	B(M1, $2_2^+ \to 2_1^+$)	B(M1, $2_3^+ \to 2_1^+$)	g_0	g_1	g_2	g_3
RVM	0.91	0.83	0.000109	0.000093	0.435	−0.089	−0.178	0.174
S1	0.91	0.83	0.000109	0.000093	0.425	−0.087	−0.174	0.170
S2	0.91	0.83	0.000109	0.000097	0.414	−0.085	−0.170	0.170
Exp. [42]	$0.91^{+0.04}_{-0.04}$	$0.83^{+0.07}_{-0.09}$	0.000109 (15)	0.000203 (23)				

Table 6. The same as Table 3 but for $\Delta \equiv$ E2/M1 mixing ratios (in eb$/\mu_N$) for ^{154}Gd.

	Exp. [41]	S1	S2	RVM	IBM [41]		Exp. [41]	S1 & S2	RVM	IBM [41]
$\Delta(2_3^+ \to 2_1^+)$	$-13.3^{+0.7}_{-0.7}$	−12.14	−12.14	-11.86	-13.3	$\Delta(3_1^+ \to 2_1^+)$	$-8.9^{+0.5}_{-0.5}$	−11.35	−11.09	-8.9
$\Delta(3_1^+ \to 4_1^+)$	$-8.9^{+0.3}_{-0.3}$	−8.29	−8.29	-8.10	-11.1	$\Delta(4_3^+ \to 4_1^+)$	$-5.5^{+0.5}_{-0.5}$	−6.34	−6.19	−7.1
$\Delta(5_1^+ \to 4_1^+)$	$-4.9^{+1.4}_{-2.9}$	−6.55	−6.55	−6.40	−4.1	$\Delta(5_1^+ \to 6_1^+)$	$-11.6^{+7.1}_{-\infty}$	−5.43	−5.30	−7.8
$\Delta(6_3^+ \to 6_1^+)$	$-4.2^{+1.8}_{-\infty}$	−4.33	−4.33	−4.23	−4.6	$\Delta(7_1^+ \to 6_1^+)$	$-2.97^{+0.50}_{-0.67}$	−4.63	−4.53	−2.2
$\Delta(7_1^+ \to 8_1^+)$	$-5.7^{+1.2}_{-1.8}$	−4.05	−4.05	−3.95	−5.9	$\Delta(2_2^+ \to 2_1^+)$	$14.4^{+2.6}_{-1.9}$	11.85	11.59	14.5
$\Delta(4_2^+ \to 4_1^+)$	$5.3^{+2.3}_{-2.3}$	6.19	6.19	6.05	6.2	$\Delta(6_2^+ \to 6_1^+)$	$2.86^{+0.33}_{-0.26}$	4.22	4.13	7.1
$\Delta(8_2^+ \to 8_1^+)$	$2.3^{+0.8}_{-0.6}$	3.21	3.21	3.14	4.4	$\Delta(10_2^+ \to 10_1^+)$	$2.4^{+1.0}_{-0.7}$	2.59	2.54	15.9
$\Delta(3_1^+ \to 2_3^+)$	$\pm(15.5^{+3.4}_{-4.4})$	24.77	24.90	21.68	28.4					

The mixing ratio $\text{B}(\text{E0}; 0_\text{i}^+ \to 0_\text{f}^+)/\text{B}(\text{E2}; 0_\text{i}^+ \to 2_1^+)$ up to the 0_4^+ state and $\rho^2(E0, 0_2^+ \to 0_1^+) \times 10^3$ are also calculated, which are shown in Table 7. It can be observed that the $\rho^2(E0, 0_2^+ \to 0_1^+) \times 10^3$ obtained from S1, S2, and the RVM is about two times larger than the experimental value, which is due to the fact that this value is almost independent of the particle-hole excitation. The main reason of why the mixing ratios of S1 differ from those of S2 is that 0_3^+ is the 2p2h state in S1, while it is the two β-phonon state in S2. Although the results of S1 seem closer to the the experimental data, the ratio $\text{B}(\text{E0}; 0_3^+ \to 0_1^+)/\text{B}(\text{E0}; 0_3^+ \to 0_2^+)$ deduced from S1 and S2 or the RVM is 27.62 and 0.020, while that deduced from the experimental data is 0.11, which shows once again that a configuration mixing of the two schemes may improve the model results.

Table 7. The same as Table 3 but for the ratio $\frac{B(E0;0_i^+\to0_f^+)}{B(E2;0_i^+\to2_1^+)}$ and $\rho^2(E0,0_2^+\to0_1^+)\times10^3$.

	Exp. [47]	S1	S2	RVM
$\frac{0_2^+\to0_1^+}{0_2^+\to2_1^+}$	0.060 (9)	0.183	0.183	0.183
$\frac{0_3^+\to0_1^+}{0_3^+\to2_1^+}$	0.112 (18)	3.377	7.716	7.716
$\frac{0_3^+\to0_2^+}{0_3^+\to2_1^+}$	1.02 (16)	0.122	392.59	392.59
$\frac{0_4^+\to0_1^+}{0_4^+\to2_1^+}$	0.80 (16)	0.142	0.234	7.716
$\rho^2(E0,0_2^+\to0_1^+)\times10^3$	89 (17); 96 (17) [43]	206.16	232.57	211.13

4. Summary

In this work, based on the collective rotor-vibrator model and the particle-plus-rotor model, multi-particle-hole excitations from a collective even-even core described by the rotor-vibrator are adopted to describe well-deformed even-even nuclei, which is a primary attempt to reveal the nature of a series of 0^+ states observed in these nuclei. It is shown that a series of experimentally observed 0^+ states in these nuclei may be interpreted as the multi-particle-hole excitations complementary to the beta and gamma vibrations described by the rotor-vibrator model. As a typical example of the model application, low-lying positive parity level energies below 1.990 MeV in the eight experimentally identified positive parity bands; a series of 0^+ excitation energies up to 0_{16}^+; and some experimentally known B(E2) values, E2 branching ratios, E2/M1 and E0/E2 mixing ratios of ^{154}Gd are fitted and compared to the experimental results.

In fitting to the level energies below 1.990 MeV in the eight experimentally identified positive parity bands in ^{154}Gd, two schemes with the 0_3^+ band head as the 2p2h state and that as the two beta-phonon state are considered. It is shown that the fitting quality of the two schemes is quite the same and much better than the original RVM, especially when higher excited 0_u^+ bands with $u=6$ and $u=7$ are involved. Although the B(E2) values of the transitions within the lowest three bands obtained from S1, S2, and the RVM are quite the same and close to the corresponding experimental data, there is noticeable deviation in the B(E2) ratios of the transitions from the 0_3^+ band to the 0_2^+ band and those from the 0_3^+ band to the ground-state band. Most of these ratios obtained from scheme 1 is too small, while they are too large in both scheme 2 and the RVM. Although the E2/M1 ratios fitted by S1, S2, and the RVM are acceptable and better than those fitted by the IBM [41], B(M1, $2_3^+\to2_1^+$) obtained from S1, S2, and the RVM is about two times smaller than the experimental value in order to obtain a best fit to the E2/M1 ratios of the inter-band transitions from the 2_3^+ band to the ground-state band. Except for B(M1, $2_3^+\to2_1^+$), the E2/M1 ratios obtained from S1 and S2 are better than those obtained from the original RVM. Deviations in the mixing ratios $B(E0;0_i^+\to0_f^+)/B(E2;0_i^+\to2_1^+)$ up to the 0_4^+ state also occur in the two schemes. Therefore, although there will be many parameters involved, a model calculation with a mixing of the two configurations determined in scheme 1 and scheme 2 may improve the results. Previously, it was pointed out that the 0_3^+ band head is a pairing isomer and can hardly be interpreted as the pure two beta-phonon state [46]. Similar conclusions on the 0_2^+ state with possible 2p2h configuration mixing were also drawn in [26,27]. As pointed out in [48], the pairing isomer can be viewed as an excited state with different deformation of the Fermi surface from that of the ground state, which is related to the so-called shape coexistence and configuration mixing [48]. Furthermore, it is concluded in [25,48] that strong proton-pair-neutron-pair correlations must be involved in low-lying 0^+ states of well-deformed even-even nuclei. The analysis of the simplified multi-particle-hole configuration mixing schemes shown in this work further confirms these conclusions, although only a part of the pairing interactions among like-nucleon pairs [25,48] are taken in effect in the 2p- and 2h-pair interaction introduced in the present work.

It is obvious that many improvements can be made in order to provide more accurate model descriptions of well-deformed nuclei. For example, rotational energies of particles and holes, and the rotation-particle and rotation-hole coupling terms neglected in the present calculation, should be included resulting in the well-known K-band mixing [49,50], with which the B(E2) values of the intra-band transitions within the 0_3^+ and 0_4^+ bands, and the related inter-band transitions and E2/M1 ratios, may be improved. Configuration mixing of the excited core with different deformation from that of the unexcited one, together with the multi-particle-hole excitations with the different deformed bases, can be considered to reveal possible shape coexistence [48] and to improve the model description of the electromagnetic transitions. A more precise description in considering all valence proton and neutron pairs confined within a deformed single-particle potential with pairing interactions is also possible. By doing so, not only can the pairing interactions among both neutron and proton pairs, together with multi-particle-hole excitations from a closed shell, be fully taken into account, but also 1^+ states formed from isovector proton–neutron pairs leading to the scissor and twist modes [9–11] lying higher in energy and not considered in this work can be produced to study the strongly enhanced M1 transitions in well-deformed nuclei. With these improvements, a model calculation for a chain of isotopes may be carried out to investigate the consistency of shape phase evolution in these nuclei [6,7,16,37]. These possible improvements will be considered in our future work. Furthermore, besides experiment in measuring E2 and M1 transition rates and mixing ratios more precisely similar to that reported in [45,46,51], two-nucleon transfer reactions in measuring 0^+ nucleon-pair transfer reaction rates in these well-deformed nuclei suggested in [25] are in demand, from which the nature of a series of excited 0^+ states can be further analyzed.

Author Contributions: Methodology, F.P.; numerical calculations and analyses, Y.W., A.L. and L.D.; writing—original draft, F.P.; writing—review and editing, J.P.D.; plus senior leadership and oversight, F.P. and J.P.D. All authors have read and agreed to the final version of the manuscript.

Funding: This research was funded by the National Natural Science Foundation of China (12175097, 12175066).

Institutional Review Board Statement: Not applicable.

Informed Consent Statement: Not applicable.

Data Availability Statement: The Mathematica code for the model calculation and the results presented are available upon request.

Conflicts of Interest: The authors have no conflict of interest.

References

1. Bohr, A.; Mottelson, B.R. *Nuclear Structure II*; Benjamin: Reading, UK, 1975.
2. Iachello, F.; Arima, A. *The Interacting Boson Model*; Cambridge University: Cambridge, UK, 1987.
3. Nikšić, T.; Vretenar, D.; Lalazissis, G.A.; Ring, P. Microscopic description of nuclear quantum phase transitions. *Phys. Rev. Lett.* **2007**, *99*, 092502. [CrossRef] [PubMed]
4. Casten, R.F. Quantum phase transitions and structural evolution in nuclei. *Prog. Part. Nucl. Phys.* **2009**, *62*, 183–209. [CrossRef]
5. Cejnar, P.; Jolie, J.; Casten, R.F. Quantum phase transitions in the shapes of atomic nuclei. *Rev. Mod. Phys.* **2010**, *82*, 2155–2212. [CrossRef]
6. Budaca, R.; Buganu, P.; Budaca, A.I. Bohr model description of the critical point for the first order shape phase transition. *Phys. Lett. B* **2018**, *776*, 26–31. [CrossRef]
7. Fortunato, L. Quantum phase transitions in algebraic and collective models of nuclear structure. *Prog. Part. Nucl. Phys.* **2021**, *121*, 103891. [CrossRef]
8. Böyükata, M.; Alonso, C.E.; Arias, J.M.; Fortunato, L.; Vitturi, A. Review of shape phase transition studies for Bose-Fermi systems: The effect of the odd-particle on the bosonic core. *Symmetry* **2021**, *13*, 215. [CrossRef]
9. Rompf, D.; Beuschel, T.; Draayer, J.P.; Scheid, W.; Hirsch, J.G. Towards understanding magnetic dipole excitations in deformed nuclei: Phenomenology. *Phys. Rev. C* **1998**, *57*, 1703–1718. [CrossRef]
10. Beuschel, T.; Hirsch, J.G.; Draayer, J.P. Scissors mode and the pseudo-SU(3) model. *Phys. Rev. C* **2000**, *61*, 054307. [CrossRef]
11. Popa, G.; Hirsch, J.G.; Draayer, J.P. Shell model description of normal parity bands in even-even heavy deformed nuclei. *Phys. Rev. C* **2000**, *62*, 064313. [CrossRef]
12. Draayer, J.P.; Weeks, K.J. Shell-model description of the low-energy structure of strongly deformed nuclei. *Phys. Rev. Lett.* **1983**, *51*, 1422–1425. [CrossRef]

13. Draayer, J.P.; Weeks, K.J. Towards a shell model description of the low-energy structure of deformed nuclei I. Even-even systems. *Ann. Phys.* **1984**, *156*, 41–47. [CrossRef]
14. Castaños, O.; Draayer, J.P.; Laschber, Y. Towards a shell-model description of the low-energy structure of deformed nuclei II. Electromagnetic properties of collective M1 bands. *Ann. Phys.* **1987**, *180*, 290–329. [CrossRef]
15. Kumar, K.; Gupta, J.B.; Hamilton, J.H. Dynamic deformation theory and multiphonon vibrational bands in ^{154}Gd. *Aust. J. Phys.* **1979**, *32*, 307–322. [CrossRef]
16. Raduta, A.A.; Faessler, A. Coherent state description of the shape phase transition in even-even Gd isotopes. *J. Phys. G Nucl. Part. Phys.* **2005**, *31*, 873–902. [CrossRef]
17. Arima, A.; Iachello, F. Interacting boson model of collective nuclear states II. The rotational limit. *Ann. Phys.* **1978**, *111*, 201–238. [CrossRef]
18. Casten, R.F. *Nuclear Structure from a Simple Perspective*, 2nd ed.; Oxford University: New York, NY, USA, 2001. [CrossRef]
19. Van Isacker, P.; Heyde, K.; Waroquier, M.; Wenes, G. An extension of the interacting boson model and its application to the even-even Gd isotope. *Nucl. Phys. A* **1982**, *380*, 383–409. [CrossRef]
20. Lipas, P.O.; Kumpulainen, J.; Hammarén, E.; Honkaranta, T.; Finger, M.; Kracikova, T.I.; Procházka, I.; Ferencei, J. Study of even Gd nuclei by decay of oriented Tb, with analysis by simple boson models. *Phys. Scr.* **1983**, *27*, 8–22. [CrossRef]
21. Lipas, P.O.; Toivonen, P.; Warner, D.D. IBA consistent-Q formalism extended to the vibrational region. *Phys. Lett. B* **1985**, *155*, 295–298. [CrossRef]
22. Han, C.S.; Chuu, D.S.; Hsieh, S.T. Effective boson number calculations near the Z = 64 subshell. *Phys. Rev. C* **1990**, *42*, 280–289. [CrossRef]
23. Nomura, K.; Otsuka, T.; Shimizu, N.; Guo, L. Microscopic formulation of the interacting boson model for rotational nuclei. *Phys. Rev. C* **2011**, *83*, 041302(R). [CrossRef]
24. van Rij, W.I.; Kahana, S.H. Low-Lying 0^+ states and (p,t) strengths in the actinides. *Phys. Rev. Lett.* **1972**, *28*, 50–54. [CrossRef]
25. Garrett, P.E. Characterization of the β vibration and 0_2^+ states in deformed nuclei. *J. Phys. G Nucl. Part. Phys.* **2001**, *27*, R1–R22. [CrossRef]
26. Sharpey-Schafer, J.F.; Mullins, S.M.; Bark, R.A.; Kau, J.; Komati, F.; Lawrie, E.A.; Lawrie, J.J.; Madiba, T.E.; Maine, P.; Minkova, A.; et al. Congruent band structures in ^{154}Gd: Configuration-dependent pairing, a double vacuum and lack of β-vibrations. *Eur. Phys. J. A* **2011**, *47*, 5. [CrossRef]
27. Sharpey-Schafer, J.F.; Madiba, T.E.; Bvumbi, S.P.; Lawrie, E.A.; Lawrie, J.J.; Minkova, A.; Mullins, S.M.; Papka, P.; Roux, D.G.; Timár, J. Blocking of coupling to the 0_2^+ excitation in ^{154}Gd by the [505]11/2$^-$ neutron in ^{155}Gd. *Eur. Phys. J. A* **2011**, *47*, 6. [CrossRef]
28. Eisenberg, J.M.; Greiner, W. *Nuclear Theory Vol. 1: Nuclear Models*, 3rd ed.; North-Holland Publishing Co.: Amsterdam, The Netherlands, 1987.
29. NuDat 2.8, National Nuclear Data Center. Brookhaven National Laboratory. Available online: http://www.nndc.bnl.gov/nudat2 (accessed on 5 October 2022).
30. Hilton, R.R.; Mang, H.J.; Ring P.; Egido, J.L.; Herold, H.; Reinecke, M.; Ruder, H.; Wunner, G. On the particle-plus-rotor model. *Nucl. Phys. A* **1981**, *366*, 365–383. [CrossRef]
31. Zhang, S.Q.; Qi, B.; Wang, S.Y.; Meng, J. Chiral bands for a quasi-proton and quasi-neutron coupled with a triaxial rotor. *Phys. Rev C* **2007**, *75*, 044307. [CrossRef]
32. Hamamoto, I. Possible presence and properties of multi-chiral-pair bands in odd-odd nuclei with the same intrinsic configuration. *Phys. Rev C* **2013**, *88*, 024327. [CrossRef]
33. Quan, S.; Liu, W.P.; Li, Z.P.; Smith, M.S. Microscopic core-quasiparticle coupling model for spectroscopy of odd-mass nuclei. *Phys. Rev C* **2017**, *96*, 054309. [CrossRef]
34. Chen, Q.B.; Lv, B.F.; Petrache, C.M.; Meng, J. Multiple chiral doublets in four-j shells particle rotor model: Five possible chiral doublets in $^{136}_{60}$Nd$_{76}$. *Phys. Lett. B* **2018**, *782*, 744–749. [CrossRef]
35. Davydov, A.S.; Chaban A. Rotation-vibration interaction in non-axial even nuclei. *Nucl. Phys.* **1960**, *20*, 499–508. [CrossRef]
36. Hara, K.; Sun, Y. Projected shell model and high-spin spectroscopy. *Int. J. Mod. Phys. E* **1995**, *4*, 637–785. [CrossRef]
37. Naz, T.; Bhat, G.H.; Jehangir, S.; Ahmad, S.; Sheikh, J.A. Microscopic description of structural evolution in Pd, Xe, Ba, Nd, Sm, Gd and Dy isotopes. *Nucl. Phys. A* **2018**, *979*, 1–20. [CrossRef]
38. Duval, P.D.; Barrett, B.R. Configuration mixing in the interacting boson model. *Phys. Lett. B* **1981**, *100*, 223–227. [CrossRef]
39. Duval, P.D.; Barrett, B.R. Quantitative description of configuration mixing in the interacting boson model. *Nucl. Phys. A* **1982**, *376*, 213–228. [CrossRef]
40. Thomas, T.; Werner, V.; Jolie, J.; Nomura, K.; Ahn, T.; Cooper, N.; Duckwitz, H.; Fitzler, A.; Fransen, C.; Gade, A.; et al. Nuclear structure of ^{96,98}Mo: Shape coexistence and mixed-symmetry states. *Nucl. Phys. A* **2016**, *947*, 203–233. [CrossRef]
41. Lipas, P.O.; Hammarén, E.; Toivonen, P. IBA-1 calculation of E2/M1 mixing ratios in ^{154}Gd. *Phys. Lett.* **1984**, *139B*, 10–14. [CrossRef]
42. Reich, C.W. Nuclear Data Sheets for A = 154. *Nucl. Data Sheets* **2009**, *110*, 2257–2532. [CrossRef]
43. Wood, J.L.; Zganjar, E.E.; De Coster, C.; Heyde, K. Electric monopole transitions from low energy excitations in nuclei. *Nucl. Phys. A* **1999**, *651*, 323–368. [CrossRef]

44. Möller, P.; Sierk, A.J.; Ichikawa T.; Sagawa, H. Nuclear ground-state masses and deformations: FRDM(2012). *At. Data Nucl. Data Tables* **2016**, *109–110*, 1–204. [CrossRef]
45. Bidaman, H. A Study on Low Spin States in ^{154}Gd Using the $(p, p'\gamma)$ Reaction. Master's Thesis, The University of Guelph, Guelph, ON, Canada, 2017. Available online: https://atrium.lib.uoguelph.ca/xmlui/handle/10214/11590 (accessed on 5 October 2022).
46. Kulp, W.D.; Wood, J.L.; Krane, K.S.; Loats, J.; Schmelzenbach, P.; Stapels, C.J.; Larimer, R.-M.; Norman, E.B. Low-energy coexisting band in ^{154}Gd. *Phys. Rev. Lett.* **2003**, *91*, 102501. [CrossRef]
47. Kibédi, T.; Spear, R.H. Electric monopole transitions between 0^+ states for nuclei throughout the periodic table. *At. Data Nucl. Data Tables* **2005**, *89*, 77–100. [CrossRef]
48. Heyde, K.; Wood, J.L. Shape coexistence in atomic nuclei. *Rev. Mod. Phys.* **2011**, *83*, 1467–1521. [CrossRef]
49. Keller, G.E.; Zganja, E.F. A note on band mixing in ^{154}Gd. *Nucl. Phys. A* **1970**, *153*, 647–651. [CrossRef]
50. Fortune, H.T. Band mixing in ^{154}Gd. *Eur. Phys. J. A* **2018**, *54*, 178. [CrossRef]
51. Girit, C.; Hamilton, W.D.; Kalfas, C.A. Multipole mixing ratios of transitions in ^{154}Gd. *J. Phys. G Nucl. Phys.* **1983**, *9*, 797–821. [CrossRef]